



Cite this: *Chem. Commun.*, 2017, 53, 2174

Received 12th December 2016,  
Accepted 23rd January 2017

DOI: 10.1039/c6cc09882g

rsc.li/chemcomm

## The small molecule JIB-04 disrupts O<sub>2</sub> binding in the Fe-dependent histone demethylase KDM4A/JMJD2A†

Barbara Cascella,<sup>ab</sup> Soon Goo Lee,<sup>b</sup> Sukrit Singh,<sup>a</sup> Joseph M. Jez\*<sup>b</sup> and Liviu M. Mirica\*<sup>a</sup>

**JIB-04, a specific inhibitor of the O<sub>2</sub>-activating, Fe-dependent histone lysine demethylases, is revealed to disrupt the binding of O<sub>2</sub> in KDM4A/JMJD2A through a continuous O<sub>2</sub>-consumption assay, X-ray crystal structure data, and molecular docking.**

Jumonji C (JmjC) domain-containing histone demethylases (HDMs) remove methyl groups from histone lysine residues through an Fe(IV)-oxo radical mechanism.<sup>1</sup> These lysine demethylases (KDMs) belong to the larger class of  $\alpha$ -ketoglutarate ( $\alpha$ KG)-dependent, non-heme iron monooxygenases and play integral roles in the maintenance of genomic integrity and transcription regulation.<sup>2,3</sup> JmjC-HDMs are considered attractive therapeutic targets as their expression is often increased in primary tumors,<sup>4</sup> but the complex histone recognition network of these enzymes makes the design of primary substrate competitive inhibitors difficult.<sup>5,6</sup> As a result, the vast majority of reported JmjC-HDM inhibitors are bidentate iron chelators acting as  $\alpha$ KG competitors.<sup>7–9</sup>

JIB-04 ((*E,Z*)-*N*-(5-chloro-pyridin-2-yl)-*N'*-(phenyl-pyridin-2-yl-methylene)-hydrazine) was the first reported specific inhibitor of JmjC-HDMs that is neither a competitor of  $\alpha$ KG nor a histone peptide mimic.<sup>10,11</sup> This pyridine hydrazone exists in two forms (Fig. 1) and displays isomer-specific inhibition with (*E*)-JIB-04 a more potent inhibitor than the *Z*-isomer. (*E*)-JIB-04 was found to reduce cancer growth *in vivo* without general toxicity, and tumour lysates of JIB-04-treated mice displayed markedly lower levels of HDM activity compared with tumour lysates of vehicle-treated mice.<sup>12</sup>

Among the JmjC-HDM isoforms, the pure H3K4me<sub>3</sub> (KDM5A) and H3K9me<sub>3</sub> demethylases (KDM4D-E) are more sensitive to JIB-04 than the H3K27 (KDM6B) and mixed H3K9/H3K36 demethylases (KDM4A-C), with reported *in vitro* IC<sub>50</sub> values

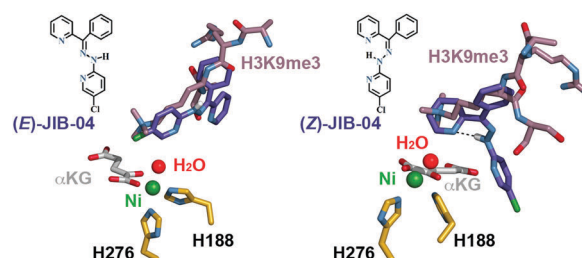


Fig. 1 JIB-04 isomers as modelled in the KDM4A active site (PDB 2Q8C); metal-coordinating residues are shown in gold.

ranging from 0.2 to 1.1  $\mu$ M. Importantly, JIB-04 does not show action against the related  $\alpha$ KG-dependent prolyl hydroxylases and ten-eleven translocation (TET) enzymes or other chromatin-modifying enzymes such as histone deacetylases.<sup>12</sup>

In competition assays, JIB-04 displayed mixed-mode inhibition with respect to  $\alpha$ KG and potentially competitive inhibition with respect to the primary histone substrate,<sup>12</sup> yet no structural data were used to supplement the competition assay findings. JIB-04 shows remarkable action in promoting cell death in cancer cells and does not alter the activities of other  $\alpha$ KG-dependent enzymes, but a thorough mechanistic understanding of the inhibitor remains to be elucidated.

Here, JIB-04's isomer-specific inhibition of JmjC-HDMs is examined through molecular modelling studies of KDM4A. A real-time O<sub>2</sub>-consumption assay was used to probe the inhibition of KDM4A by JIB-04 at varying concentrations of O<sub>2</sub>, and JIB-04's inhibitory strength increases in low-oxygen environments, suggesting that the hypoxic environment of the cancer cells contributes to the efficacy of JIB-04 *in vivo*. Finally, a 2.75 Å crystal structure of KDM4A in complex with Ni(II) was formed in the presence of JIB-04, and modelling of (*E*)-JIB-04 within the complex suggests that it works by disrupting the binding of O<sub>2</sub> and histone JmjC-HDM substrates.

JIB-04 was docked into a crystal structure of KDM4A in complex with  $\alpha$ KG and an H3K9me<sub>3</sub> peptide (sequence ARKS) without ligand-guided assistance using OpenEye's FRED docking program,

<sup>a</sup> Department of Chemistry, Washington University, St. Louis, Missouri 63130, USA.  
E-mail: mirica@wustl.edu

<sup>b</sup> Department of Biology, Washington University, St. Louis, Missouri 63130, USA.  
E-mail: jjez@wustl.edu

† Electronic supplementary information (ESI) available: Experimental and computational details, X-ray crystallographic data, and MALDI-TOF mass spectrometry data. See DOI: 10.1039/c6cc09882g

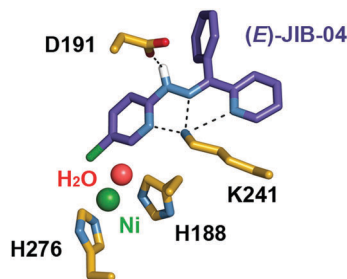


Fig. 2 Predicted hydrogen bonding between (*E*)-JIB-04 and KDM4A residues, highlighted with dashes.

meaning that the bound conformation of the peptide substrate was not used to guide the modelling of either isomer (Fig. 1 and 2).<sup>‡</sup> The lowest-energy poses are shown, with the aromatic moieties of (*E*)-JIB-04 oriented in a fashion that mimics the projection of the H3K9me<sub>3</sub> substrate toward the metal centre in the KDM4A active site, while an intramolecular hydrogen bond between the hydrazone and pyridine (H–N···N distance of 2.8 Å) limits the protein-binding opportunities of (*Z*)-JIB-04.

A closer look at the predicted binding of (*E*)-JIB-04 reveals hydrogen bonds between Lys 241 and the N atoms of the two pyridine and one hydrazone groups (H<sub>3</sub>N<sup>+</sup>···N distances of 2.7, 3.1, and 2.7 Å, respectively; H<sub>3</sub>N<sup>+</sup>···N distances between (*Z*)-JIB-04 and Lys 241 are approximately an Ångström further in each case). This hydrogen bonding is significant since Lys 241 is proposed to be essential in recruiting O<sub>2</sub> to the active site of KDM4A.<sup>6</sup> An additional hydrogen bond is predicted to form between the hydrazone and the carboxylate of Asp 191 (N–H···O distance of 2.4 Å). Similar to the binding of the H3K36me<sub>3</sub> peptide in the KDM4A active site,<sup>6</sup> we find no evidence of hydrophobic interactions to stabilize JIB-04 binding, as the nearest aromatic residue, Tyr 175, is slightly displaced and over 5 Å away.

The initial report of JIB-04 found a half-maximal inhibitory concentration (IC<sub>50</sub>) of 445 nM when testing a KDM4A concentration of 206 nM, but the *in vitro* assay conditions were not reported in detail.<sup>§</sup> Herein, an O<sub>2</sub>-consumption assay was used to test for inhibition of KDM4A using JIB-04 synthesized as a monohydrate.<sup>12,18</sup> Pre-incubation of the holoenzyme with JIB-04 before the start of the reaction was necessary for notable enzyme inhibition, and this was confirmed by a MALDI-TOF mass spectrometry assay (Fig. S1, ESI<sup>†</sup>). KDM4A inhibition was screened at varying levels of O<sub>2</sub> using a Clark oxygen electrode to track enzymatic activity in real-time (Fig. 3).<sup>19</sup> Briefly, a solution of αKG (300 μM), ascorbic acid (500 μM), H3<sub>(7–14)</sub>K9me<sub>3</sub> (100 μM), HEPES (pH 7.5, 50 mM), and Tween-20 (0.1%) was equilibrated under varying partial pressures of O<sub>2</sub>; outside the reaction vessel, KDM4A (2 μM, reconstituted with one equivalent Fe(II)) was incubated with JIB-04 in DMSO (0–20 μM; higher concentrations could not be tested due to the limited solubility of JIB-04). The injection of the HDM-Fe(II)-JIB-04 complex into the reaction chamber marked the start of the reaction. Enzyme inhibition was tested at three concentrations of O<sub>2</sub>: 60 μM (≈K<sub>m</sub>(O<sub>2</sub>) for KDM4A), 258 μM (air-saturated water), and 1200 μM (O<sub>2</sub>-saturated water).<sup>19</sup> IC<sub>50</sub> plots and values at the three concentrations of O<sub>2</sub> are shown in Fig. 3.

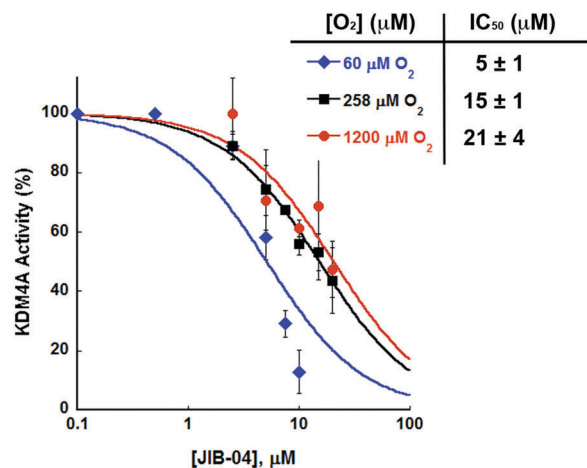


Fig. 3 Inhibition of KDM4A by JIB-04 as tested at three concentrations of O<sub>2</sub>.

With decreasing O<sub>2</sub> concentrations we find decreasing IC<sub>50</sub> values, and thus an increased potency of JIB-04 inhibition. While there is little difference between KDM4A's relative activity at the three O<sub>2</sub> concentrations with 2.5 μM JIB-04, we find substantial differences in activity at inhibitor concentrations ≥7.5 μM, with total enzyme inactivation at JIB-04 concentrations higher than 10 μM only in the low-O<sub>2</sub> environment. Based on these data, we would expect increased inhibitor efficacy at concentrations of O<sub>2</sub> like those found in hypoxic tissues (median pO<sub>2</sub> ≈ 2–10 mmHg or ≈ 4–20 μM);<sup>20</sup> however, KDM4A activity is difficult to accurately monitor below 60 μM O<sub>2</sub>. The nearly 3-fold difference in IC<sub>50</sub> values between 258 and 60 μM O<sub>2</sub> suggests that JIB-04 disrupts the binding of O<sub>2</sub> within the KDM4A active site, while the similar IC<sub>50</sub> values at 258 μM and 1200 μM could be expected if JIB-04 is competitive with respect to O<sub>2</sub>, since 258 μM and 1200 μM are significantly higher than the K<sub>m</sub>(O<sub>2</sub>) value for KDM4A.<sup>19</sup> Notably, KDM4A is not the most affected target of JIB-04 since it is a mixed H3K9/H3K36 demethylase; testing the pure H3K4 and H3K9 KDMs could help to confirm that the drug exhibits a range of potencies in low- and high-O<sub>2</sub> environments.

We were successful in crystallizing the catalytic JmjC and JmjN domains of KDM4A in complex with Ni(II) and in the presence of (*E*)-JIB-04, but not in the presence of (*E*)-JIB-04 and αKG or *N*-oxalylglycine (NOG).<sup>¶</sup> The refinement of the crystallographic structure to 2.75 Å resolution revealed the electron density of the inhibitor to be unclear and so the molecular modelling of (*E*)-JIB-04 into the KDM4A-Ni(II) complex was performed using AutoDock Vina (ver. 1.1.2).<sup>‖</sup> The lowest-energy pose (Fig. 4) has an apparent binding affinity of about 2 kcal mol<sup>-1</sup> lower in energy than the most favourable poses in KDM4A-Ni(II)-αKG (PDB 5TVR), KDM4A-Ni(II)-NOG (PDB 2OQ7), and KDM4A-Ni(II)-αKG-H3K9me<sub>3</sub> (PDB 2Q8C) complexes, and approximately equal in energy to the binding affinity found for (*E*)-JIB-04 modelled in JARID1B/KDM5B (PDB 5A1F), the most sensitive JmjC-HDM to JIB-04 in *in vitro* studies (Table S1, ESI<sup>†</sup>).<sup>12,22,23</sup> Taken together, these data indicate that (*E*)-JIB-04 has likely influenced the architecture of the KDM4A active site in the 2.75 Å structure.

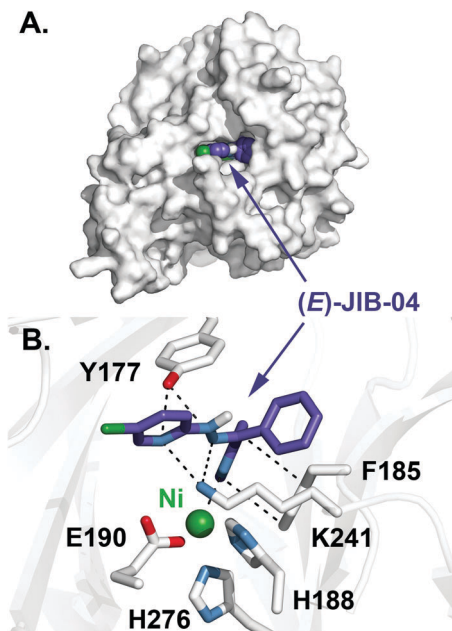


Fig. 4 Structure of KDM4A in complex with Ni(II) and the lowest-energy (*E*)-JIB-04 conformer. (A) Surface view of KDM4A with a space-filling model of (*E*)-JIB-04. (B) Interactions of (*E*)-JIB-04 with KDM4A active site residues highlighted by dashes.

In the complex, (*E*)-JIB-04 is predicted to form two hydrogen bonds with Tyr 177 (HO...N distances of 3.1 and 3.2 Å), a residue involved in the binding of the trimethylammonium group of the enzyme's histone substrate (Fig. 4B);<sup>5,17</sup> this interaction is in line with earlier findings pointing to (*E*)-JIB-04 acting competitively with respect to the primary substrate. At least one hydrogen bond with Lys 241 forms (H<sub>3</sub>N<sup>+</sup>...N distance of 3.1 Å, with a possible second interaction at 3.7 Å), and this residue is responsible for the recruitment of O<sub>2</sub> in KDM4A.<sup>6</sup> Additional sources of stability in this model come from a  $\pi$ - $\pi$  stacking interaction with Phe 185 (4 Å) and possible chelation of the metal centre by the unsubstituted pyridine nitrogen (2.7 Å), which is not possible for the *Z*-isomer due to its intramolecular hydrogen bond. As shown in the surface view (Fig. 4A), the hydrazone N-H group is solvent accessible and available for hydrogen bonding. While the predicted binding mode of (*E*)-JIB-04 in this structure is different from that found with PDB 2Q8C docking studies (Fig. 1), both models have (*E*)-JIB-04 interacting with Lys 241 through hydrogen bonding. This, in conjunction with the O<sub>2</sub>-consumption assay results, indicates that (*E*)-JIB-04 disrupts the binding of O<sub>2</sub> in the KDM4A active site.

The 2.75 Å KDM4A-Ni(II) structure shows a high degree of similarity to the 2.05 Å structure KDM4A-Ni(II)- $\alpha$ KG-H3K9me<sub>3</sub> (PDB 2Q8C) when the two are overlaid (Fig. 5A). However, there are notable shifts in positioning of the metal centre as well as metal-coordinating residues His 188, His 276, and Glu 190 (Fig. 5B), with Ni(II) in the 2.75 Å structure positioned about 1 Å closer to the unsubstituted pyridine nitrogen of (*E*)-JIB-04, which overlaps with the binding site of  $\alpha$ KG in 2Q8C. These active site residue shifts are likely due to the presence of  $\alpha$ KG in PDB 2Q8C rather than the presence of the histone peptide substrate,

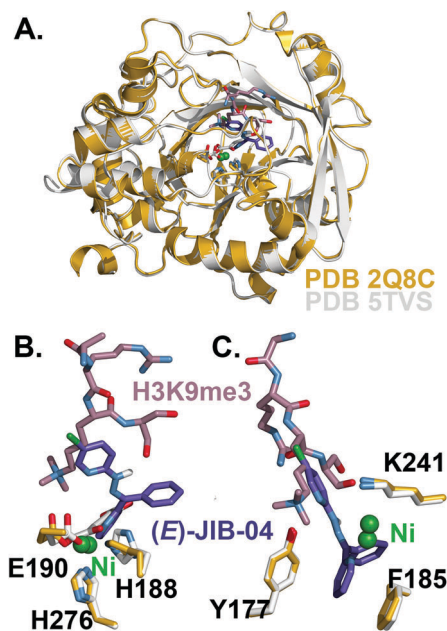


Fig. 5 Structure comparison of PDB 2Q8C (in gold) and KDM4A-Ni(II) (in white) with (*E*)-JIB-04 docked. (A) Overlay of the two structures shows a high degree of structural similarity. (B) Metal centre and metal-coordinating residue displacements in the two active sites, with (*E*)-JIB-04 in  $\alpha$ KG's binding site. (C) (*E*)-JIB-04-binding residues show little displacement between the two structures.

since overlaying the 2.75 Å structure with a 2.1 Å KDM4A-Ni(II)- $\alpha$ KG (PDB 5TVR) structure shows a similar degree of active site residue displacement (Fig. S2, ESI<sup>†</sup>). This could be an indication that the inhibitor can alter the binding of the co-substrate, since earlier studies found mixed-mode inhibition of (*E*)-JIB-04 with respect to  $\alpha$ KG.<sup>12</sup> In the histone- and O<sub>2</sub>-binding portions of the active site, only slight differences in KDM4A residues are found between the two crystal structures (Fig. 5C).

In conclusion, the structural data reported here, in combination with computational docking, indicate that (*E*)-JIB-04 interacts with Lys 241 and Tyr 177 through hydrogen bonding, thus disrupting the binding of O<sub>2</sub> and histone substrates in the KDM4A active site. Additionally, the inhibitor may chelate the metal centre, thereby altering the binding ability of the co-substrate  $\alpha$ KG. Importantly, a continuous O<sub>2</sub>-consumption assay reveals that JIB-04 is a more effective inhibitor of KDM4A in low-O<sub>2</sub> environments, a further indication that the inhibitor is competitive with respect to O<sub>2</sub>. We propose that JIB-04's selective anticancer properties, as evidenced by reduced tumour growth without general toxicity in JIB-04-treated mice,<sup>12</sup> are in part due to its disruption of O<sub>2</sub>-binding in JmJc-HDM active sites. While the O<sub>2</sub> affinities of most JmJc-HDMs are unknown, the KDM4 sub-family exhibits low apparent affinities for O<sub>2</sub>, with  $K_m$ (O<sub>2</sub>) values close to and above the O<sub>2</sub> levels in well-oxygenated tissues.<sup>19</sup> It is therefore likely that it is the low-oxygen environment of the cancer cell which allows JIB-04 to exhibit specificity of action in cancer cells over healthy cells. Our biochemical studies prompt further investigation to find how JIB-04 influences the activities of  $\alpha$ KG-dependent HDMs in cell culture under varying tensions

of O<sub>2</sub>. Overall, these studies suggest that the development of specific inhibitors for JmjC-HDMs should focus on compounds that act as competitive inhibitors with respect to more than one substrate, preferably both O<sub>2</sub> and the histone substrate.

## Notes and references

‡ Ten thousand conformers of the *E*- and *Z*-isomers were generated using OMEGA following minimization by SZYBKI.<sup>24,25</sup> Conformers were modelled into the active site using the Poisson–Boltzmann solvation method at 310 K, taking into account cavity solvation energies. All renderings were generated using PyMOL.<sup>26</sup>

§ In the original report, neither the concentration nor the length of H3K9me<sub>3</sub> peptide used was specified; assuming the use of H3<sub>(7–14)</sub>K9me<sub>3</sub>, a 1:6.5 ratio of KDM4A:H3K9me<sub>3</sub> is calculated (400 ng KDM4A ≈ 9.1 × 10<sup>−9</sup> mmol, 50 ng H3<sub>(7–14)</sub>K9me<sub>3</sub> ≈ 5.9 × 10<sup>−8</sup> mmol); the 1:50 KDM4A:H3K9me<sub>3</sub> ratio used here would lead to a higher IC<sub>50</sub> value since (*E*)-JIB-04 is competitive with respect to the histone peptide.

¶ KDM4A was expressed and purified as previously described, with size-exclusion chromatography (Sephadex 75) as an additional, and final, purification step.<sup>19</sup> KDM4A (12.0 mg mL<sup>−1</sup>) was pre-incubated with 750 μM JIB-04 and 300 μM NiCl<sub>2</sub> for 30 min before crystallization. Protein crystals were grown using the vapour diffusion method in hanging-drops of a 1:1 mixture of protein and crystallization buffer (17.5% PEG-3350 and 0.1 M citrate pH 6.0). Diffraction data were collected at beamline 19-ID of the Argonne National Lab Advanced Photon Source. HKL300022<sup>27</sup> was used for indexing, integration, and scaling of diffraction data. The crystal structure of KDM4A<sub>Ni(II)</sub> was determined *via* a molecular replacement using PHASER23<sup>28</sup> and the structure of the catalytic core of JMJD2A (PDB 2GP3)<sup>29</sup> with ligands removed as the search model. Manual model building and refinement were performed in COOT<sup>30</sup> and PHENIX,<sup>31</sup> respectively. Data collection and refinement statistics are summarized in Table S2 (ESI<sup>†</sup>). Coordinates and structure factors for the KDM4A<sub>Ni(II)</sub> complex have been deposited in the Protein Data Bank (5TVS).

|| The ligand was generated using ChemDraw 3D and was energy minimized. Twenty low-energy poses of (*E*)-JIB-04 were modelled in the protein complex using a grid box of 36 × 38 × 32 Å and the level of exhaustiveness set to 40.

- 1 M. Costas, M. P. Mehn, M. P. Jensen and L. Que Jr., *Chem. Rev.*, 2004, **104**, 939–986.
- 2 S. R. Bhaumik, E. Smith and A. Shilatifard, *Nat. Struct. Mol. Biol.*, 2007, **14**, 1008–1016.
- 3 R. J. Klose, E. M. Kallin and Y. Zhang, *Nat. Rev. Genet.*, 2006, **7**, 715–727.
- 4 J. W. Højfeldt, K. Agger and K. Helin, *Nat. Rev. Drug Discovery*, 2013, **12**, 917–930.
- 5 S. S. Ng, K. L. Kavanagh, M. A. McDonough, D. Butler, E. S. Pilka, B. M. R. Lienard, J. E. Bray, P. Savitsky, O. Gileadi, F. von Delft, N. R. Rose, J. Offer, J. C. Scheinost, T. Borowski, M. Sundstrom, C. J. Schofield and U. Oppermann, *Nature*, 2007, **448**, 87–91.
- 6 Z. Chen, J. Zang, J. Kappler, X. Hong, F. Crawford, Q. Wang, F. Lan, C. Jiang, J. Whetstine and S. Dai, *Proc. Natl. Acad. Sci. U. S. A.*, 2007, **104**, 10818–10823.
- 7 K.-H. Chang, O. N. F. King, A. Tumber, E. C. Y. Woon, T. D. Heightman, M. A. McDonough, C. J. Schofield and N. R. Rose, *ChemMedChem*, 2011, **6**, 759–764.
- 8 O. N. F. King, X. S. Li, M. Sakurai, A. Kawamura, N. R. Rose, S. S. Ng, A. M. Quinn, G. Rai, B. T. Mott and P. Beswick, *PLoS One*, 2010, **5**, e15535.
- 9 N. R. Rose, S. S. Ng, J. Mecinovic, B. M. R. Lienard, S. H. Bello, Z. Sun, M. A. McDonough, U. Oppermann and C. J. Schofield, *J. Med. Chem.*, 2008, **51**, 7053–7056.
- 10 E. C. Y. Woon, A. Tumber, A. Kawamura, L. Hillringhaus, W. Ge, N. R. Rose, J. H. Y. Ma, M. C. Chan, L. J. Walport, K. H. Che, S. S. Ng, B. D. Marsden, U. Oppermann, M. A. McDonough and C. J. Schofield, *Angew. Chem., Int. Ed.*, 2012, **51**, 1631–1634.
- 11 B. Lohse, A. L. Nielsen, J. B. L. Kristensen, C. Helgstrand, P. A. C. Cloos, L. Olsen, M. Gajhede, R. P. Clausen and J. L. Kristensen, *Angew. Chem., Int. Ed.*, 2011, **123**, 9266–9269.
- 12 L. Wang, J. Chang, D. Varghese, M. Dellinger, S. Kumar, A. M. Best, J. Ruiz, R. Bruick, S. Peña-Llopis, J. Xu, D. J. Babinski, D. E. Frantz, R. A. Brekken, A. M. Quinn, A. Simeonov, J. Easmon and E. D. Martinez, *Nat. Commun.*, 2013, **4**, 2035.
- 13 G. B. McGaughey, R. P. Sheridan, C. I. Bayly, J. C. Culberson, C. Kreatsoulas, S. Lindsley, V. Maiorov, J.-F. Truchon and W. D. Cornell, *J. Chem. Inf. Model.*, 2007, **47**, 1504–1519.
- 14 M. McGann, *J. Chem. Inf. Model.*, 2011, **51**, 578–596.
- 15 M. McGann, *J. Comput.-Aided Mol. Des.*, 2012, **26**, 897–906.
- 16 B. P. Kelley, S. P. Brown, G. L. Warren and S. W. Muchmore, *J. Chem. Inf. Model.*, 2015, **55**, 1771–1780.
- 17 J. F. Couture, E. Collazo, P. A. Ortiz-Tello, J. S. Brunzelle and R. C. Trievel, *Nat. Struct. Mol. Biol.*, 2007, **14**, 689–695.
- 18 J. Easmon, G. Heinisch, G. Pürstinger, T. Langer, J. K. Österreicher, H. H. Grunicke and J. Hofmann, *J. Med. Chem.*, 1997, **40**, 4420–4425.
- 19 B. Cascella and L. M. Mirica, *Biochemistry*, 2012, **51**, 8699–8701.
- 20 P. Vaupel, A. Mayer and M. Höckel, *Methods Enzymol.*, 2004, **381**, 335–354.
- 21 O. Trott and A. Olson, *J. Comput. Chem.*, 2010, **31**, 455–461.
- 22 J. R. Horton, A. K. Upadhyay, H. H. Qi, X. Zhang, Y. Shi and X. Cheng, *Nat. Struct. Mol. Biol.*, 2010, **17**, 38–43.
- 23 C. Johansson, S. Velupillai, A. Tumber, A. Szykowska, E. S. Hookway, R. P. Nowak, C. Strain-Damerell, C. Gileadi, M. Philpott, N. Burgess-Brown, N. Wu, J. Kopec, A. Nuzzi, H. Steuber, U. Egner, V. Badock, S. Munro, N. B. LaThangue, S. Westaway, J. Brown, N. Athanasou, R. Prinjha, P. E. Brennan and U. Oppermann, *Nat. Chem. Biol.*, 2016, **12**, 539–545.
- 24 P. C. D. Hawkins, A. G. Skillman, G. L. Warren, B. A. Ellingson and M. T. Stahl, *J. Chem. Inf. Model.*, 2010, **50**, 572–584.
- 25 T. A. Halgren, *J. Comput. Chem.*, 1996, **17**, 490–519.
- 26 The PyMOL Molecular Graphics System, Version 1.8, Schrodinger, LLC, 2015.
- 27 W. Minor, M. Cymborowski, Z. Otwinowski and M. Chruszcz, *Acta Crystallogr., Sect. D: Biol. Crystallogr.*, 2006, **62**, 859–866.
- 28 A. J. McCoy, R. W. Grosse-Kunstleve, P. D. Adams, M. D. Winn, L. C. Storoni and R. J. Read, *J. Appl. Crystallogr.*, 2007, **40**, 658–674.
- 29 Z. Chen, J. Zang, J. Whetstine, X. Hong, F. Davrazou, T. G. Kutateladze, M. Simpson, Q. Mao, C. H. Pan, S. Dai, J. Hagman, K. Hansen, Y. Shi and G. Zhang, *Cell*, 2006, **125**, 691–702.
- 30 P. Emsley and K. Cowtan, *Acta Crystallogr., Sect. D: Biol. Crystallogr.*, 2004, **60**, 2126–2132.
- 31 P. D. Adams, P. V. Afonine, G. Bunkóczi, V. B. Chen, I. W. Davis, N. Echols, J. J. Headd, L.-W. Hung, G. J. Kapral and R. W. Grosse-Kunstleve, *Acta Crystallogr., Sect. D: Biol. Crystallogr.*, 2010, **66**, 213–221.